EARTH SURFACE PROCESSES AND LANDFORMS
Earth Surf. Process. Landforms **35**, 941–951 (2010)
Published in 2010 by John Wiley & Sons, Ltd.
Published online 1 February 2010 in Wiley InterScience
(www.interscience.wiley.com) DOI: 10.1002/esp.1982

Catastrophic rock avalanche 3600 years BP from El Capitan, Yosemite Valley, California†

Greg M. Stock[1,*] and Robert A. Uhrhammer[2]
[1] National Park Service, Yosemite National Park, Resources Management and Science, 5083 Foresta Road, PO Box 700, El Portal, California 95318, USA
[2] Berkeley Seismological Laboratory, University of California, 215 McCone Hall #4760, Berkeley, California 94720, USA

Received 14 August 2009; Revised 19 November 2009; Accepted 30 November 2009

*Correspondence to: G. M. Stock, National Park Service, Yosemite National Park, Resources Management and Science, 5083 Foresta Road, PO Box 700, El Portal, California 95318, USA. E-mail: greg_stock@nps.gov

ESPL
Earth Surface Processes and Landforms

ABSTRACT: Large rock slope failures from near-vertical cliffs are an important geomorphic process driving the evolution of mountainous landscapes, particularly glacially steepened cliffs. The morphology and age of a $2{\cdot}19 \times 10^6$ m^3 rock avalanche deposit beneath El Capitan in Yosemite Valley indicates a massive prehistoric failure of a large expanse of the southeast face. Geologic mapping of the deposit and the cliff face constrains the rock avalanche source to an area near the summit of ~$8{\cdot}5 \times 10^4$ m^2. The rock mass free fell ~650 m, reaching a maximum velocity of 100 m s^{-1}, impacted the talus slope and spread across the valley floor, extending 670 m from the base of the cliff. Cosmogenic beryllium-10 exposure ages from boulders in the deposit yield a mean age of $3{\cdot}6 \pm 0{\cdot}2$ ka. The ~13 kyr time lag between deglaciation and failure suggests that the rock avalanche did not occur as a direct result of glacial debuttressing. The ~3·6 ka age for the rock avalanche does coincide with estimated late Holocene rupture of the Owens Valley fault and/or White Mountain fault between 3·3 and 3·8 ka. The coincidence of ages, combined with the fact that the most recent (AD 1872) Owens Valley fault rupture triggered numerous large rock falls in Yosemite Valley, suggest that a large magnitude earthquake (≥M7.0) centered in the south-eastern Sierra Nevada may have triggered the rock avalanche. If correct, the extreme hazard posed by rock avalanches in Yosemite Valley remains present and depends on local earthquake recurrence intervals. Published in 2010 by John Wiley & Sons, Ltd.

KEYWORDS: landslide; rock fall; seismic trigger; cosmogenic nuclide dating

Introduction

Large rock slope failures are among the most effective of the processes shaping mountainous landscapes. Although these events have relatively low frequencies, they move large masses of material over long distances, performing in geologically instantaneous time the amount of work accomplished over millennia by more frequent but smaller magnitude surface processes. Large rock slope failures are responsible for large proportions of mountain erosion, and are thus important events in controlling long-term rates of landscape evolution in mountainous regions (Hovius and Stark, 2007). Because earthquakes and climate events (in the form of glacial retreat or intense precipitation events) are common triggers of large rock slope failures, their study can elucidate the tectonic and climatic forces controlling hillslope adjustment to topographic relief (Korup *et al.*, 2007). Large rock slope failures from near vertical cliffs, under-represented in geologic study, are an important means by which glacially-modified landscapes evolve.

Yosemite Valley is a ~1 km deep canyon carved into granitic rocks of the Sierra Nevada batholith (Bateman, 1992). The valley has fluvial origins, but was substantially deepened and widened by Pleistocene glacial erosion (Matthes, 1930; Gutenberg *et al.*, 1956; Huber, 1987). Because the granitic rocks in the Yosemite region are relatively massive with high rock mass strength values, they support extremely steep, even overhanging, rock faces such as El Capitan, Half Dome, Royal Arches, and Cathedral Rocks. Yosemite Valley was most recently glaciated during the Last Glacial Maximum (LGM), locally termed the Tioga Glaciation, which lasted from ~28–14 ka in the Sierra Nevada (Matthes, 1930; Huber, 1987; Phillips *et al.*, 1996, 2009; Clark *et al.*, 2003).

The glacially steepened cliffs of Yosemite Valley experience frequent rock falls. A database extending from AD 1857 to the present documents over 600 rock falls or other forms of slope movement, such as rock slides and debris flows, in Yosemite National Park (Wieczorek and Snyder, 2004, and subsequent observations). The vast majority of these events were rock falls and rock slides in Yosemite Valley, with individual rock fall

volumes up to ~600,000 m^3. Failures often occur as planar or slab failures along surface-parallel sheeting joints. Analysis of the rock-fall database reveals a range of triggers, including precipitation, freeze–thaw, and thermal stresses, although >50% of documented rock falls lack recognized triggering mechanisms (Wieczorek and Jäger, 1996; Wieczorek and Snyder, 2004).

Earthquakes have triggered at least 20 historic rock falls in Yosemite Valley, for a cumulative volume of ~67,400 m^3 (Wieczorek and Jäger, 1996; Wieczorek and Snyder, 2004). The 25–27 May 1980 earthquakes centered near Mammoth Lakes, with magnitudes as great as M 6·5, triggered thousands of rock falls and rock slides in the Sierra Nevada (Harp *et al.*, 1984) and at least nine rock falls in Yosemite Valley (Wieczorek and Jäger, 1996; Wieczorek and Snyder, 2004). The 26 March 1872 Owens Valley earthquake, one of the largest historic earthquakes in California (M 7·5; Beanland and Clark, 1994), triggered at least five large (up to 36,000 m^3) rock falls in Yosemite Valley (Wieczorek and Snyder, 2004), which is located 180 km north-west of the rupture. The conservationist John Muir famously described one of the resulting rock falls:

> At half past two o'clock of a moonlit morning in March, I was awakened by a tremendous earthquake . . . The shocks were so violent and varied, and succeeding one another so closely . . . it seemed impossible that the high cliffs of the Valley should escape being shattered . . . Then suddenly . . . there came a tremendous roar. The Eagle Rock on the south wall, about half a mile up the Valley, gave way and I saw it falling in thousands of great boulders . . . pouring to the Valley floor in a free curve luminous from friction, making a terribly sublime spectacle – an arc of glowing, passionate fire, fifteen hundred feet span . . . (Muir, 1912).

Wieczorek (2002) estimated that this rock fall, originating from the southern slope of Yosemite Valley between Glacier Point and Sentinel Rock, had an approximate volume of 20,000 m^3.

Beyond historical timescales, longer-term rock-fall activity in Yosemite is reflected in the large volumes of talus that have accumulated beneath the cliffs since retreat of the LGM glaciers (Wieczorek and Jäger, 1996; Moore *et al.*, 2009). Active talus slopes in Yosemite Valley are commonly 100 m thick (over 200 m thick in places) and extend horizontally 100 m or more beyond the base of cliffs. The distal edge of active talus slopes represents the limit that typical rock falls extend beyond cliff faces (Wieczorek *et al.*, 1999).

At five locations in Yosemite Valley, rock debris has traveled far beyond the distal edge of active talus slopes and out onto the valley floor (Wieczorek *et al.*, 1999). These deposits have been interpreted as rock avalanches based on their size and runout distances (Wieczorek *et al.*, 1999; Wieczorek, 2002). Rock avalanches are massive slope failures consisting of mostly dry rock debris and generally characterized by distinctive morphologies, long runout distances relative to their fall heights, velocities of tens of meters per second, and volumes exceeding $1{\cdot}0 \times 10^6$ m^3 (Shreve, 1968; Scheidegger, 1973; Hsu, 1975; Nicoletti and Sorriso-Valvo, 1991; Davies and McSaveney, 1999; Strom and Korup, 2006; Mitchell *et al.*, 2007; Shea and van Wyk de Vries, 2008). Given their large size, rock avalanches are an important geomorphic process driving landscape evolution in Yosemite Valley. With nearly four million visitors to Yosemite National Park annually, rock avalanches also pose an extreme hazard that warrants additional investigation. Here we present research results on the magnitude, timing, and potential triggering mechanisms of a prominent rock avalanche beneath the near-vertical south-east face of El Capitan.

El Capitan Meadow Rock Avalanche

Rising 940 m above the floor of Yosemite Valley (mean elevation 1208 m), with a vertical to overhanging face up to 895 m tall, El Capitan is among the largest and most widely-recognized granitic rock faces in the world (Figure 1). Historically, there have been relatively few rock falls documented from El Capitan (Wieczorek and Snyder, 2004, and subsequent observations). However, this is at least in part due to the fact that rock-fall reporting rates are comparatively low in this undeveloped area. A large apron of active talus beneath El Capitan, ranging from 45 to 225 m high and extending horizontally outward from the cliff face 160–400 m, is evidence of extensive post-glacial rock-fall activity (Figures 2, 3).

Below the south-east face of El Capitan, a tongue-shaped deposit of rock debris extends well beyond the distal edge of the active talus slope (Figures 2 and 3). Matthes (1930) described that deposit as follows:

> . . . the most remarkable body of earthquake débris is that which lies in front of El Capitan – not the talus of blocks that slopes steeply from the cliff to the valley floor, but the much vaster hummocky mass, partly obscured by a growth of trees and brush, that sprawls nearly half a mile out into the valley. There can be no doubt that it is the product in the main of one colossal avalanche that came down from the whole height of the cliff face – probably the most spectacular rock avalanche that has fallen in the Yosemite Valley since the glacial epoch . . . the quantity of débris that fell in this stupendous earthquake avalanche is so great . . . that its removal doubtless altered appreciably the contour and appearance of El Capitan.

This deposit, termed the El Capitan Meadow rock avalanche (Wieczorek *et al.*, 1999), is well resolved in a 1 m digital elevation model (DEM) and shaded relief model (Figure 2) created from filtered airborne LiDAR data. The rock avalanche deposit has a lobate morphology where it emerges from

Figure 1. The south-east face of El Capitan in Yosemite Valley. The 'Nose' forms the curving arête separating the sunlit and shaded parts of the cliff. The 'North America Wall' is the concave section of wall to the right of the Nose, marked by a mafic dike in the shape of North America. The height of the cliff face between the Nose and the North America Wall is ~800 m. The white dashed line marks the extent of the El Capitan Meadow rock avalanche deposit.

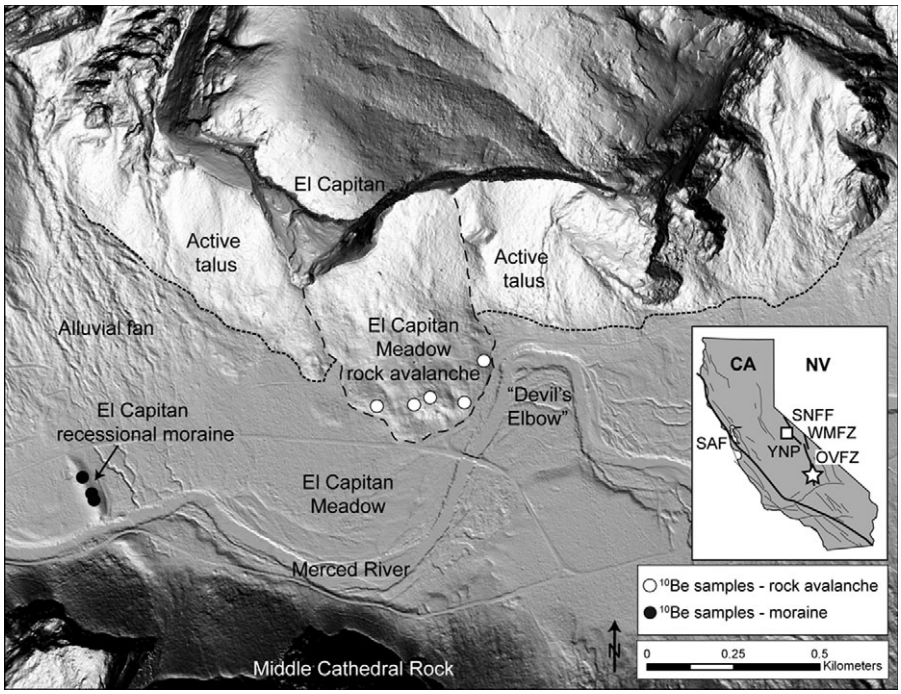

Figure 2. Shaded relief model produced from filtered LiDAR DEM of EI Captain in Yosemite Valley. Black dashed line delineates the extent of the El Capitan Meadow rock avalanche and black dotted line delineates the distal edge of the active talus slope. Inset shows the major tectonic structures of California, including (in bold lines) the San Andreas Fault (SAF), Owens Valley Fault Zone (OVFZ), White Mountain Fault Zone (WMFZ), and Sierra Nevada Frontal Fault (SNFF). The white square marks the location of Yosemite National Park, and the white star marks the epicenter of the AD 1872 Owens Valley earthquake.

Figure 3. The El Capitan Meadow rock avalanche as seen from ~440 m above the base of the south-east face of El Capitan, near the inferred minimum elevation of the rock avalanche source area. The rock avalanche deposit (white dashed line) has a runout distance of ~670 m from the base of the cliff and extends ~395 m beyond the base of the active talus slope (white dotted line) onto the valley floor. Photo by Lincoln Else.

Table I. Physical parameters for the El Capitan Meadow rock avalanche

Parameter	Value
Area of deposit	$2{\cdot}71 \times 10^3$ m^2
Volume of deposit	$2{\cdot}19 \times 10^6$ m^3
Volume of intact rock	$1{\cdot}64 \times 10^6$ m^3
Rock wall source	
Source area	~$8{\cdot}5 \times 10^4$ m^2
Maximum source elevation (m)	2155
Minimum source elevation (m)	~1840
Mean slope of source area (°)	87
Exposure	Southeast
Rock type	Granite, granodiorite, minor diorite
Run out of debris	
Maximum elevation of deposit (m)	1425
Minimum elevation of deposit (m)	1204
Maximum vertical drop (m)	950
Maximum horizontal travel (m)	710
Energy slope (°)	54
Fahrböschung (°)	53
Coefficient of friction (H/L)	1·34
Total emplacement time (s)	24·1
Maximum velocity during emplacement (m s^{-1})	100

beneath the active talus slope and extends out onto the nearly horizontal valley floor (Figure 2). The deposit has a total runout distance of 710 m from the top of the cliff, and a runout distance of 670 m from the base of the cliff. It extends roughly halfway across the width of Yosemite Valley, causing the Merced River to divert sharply to the south at a location known as the 'Devil's Elbow' (Figure 2). Approximately 275 m of the total runout distance is beneath the active talus slope, with the remaining 395 m extending beyond the base of the active talus slope and onto the valley floor. This distal portion, where the morphology is best resolved, has a minimum width of 405 m and a maximum width of 455 m (Table 1). The deposit has a planimetric surface area of $2{\cdot}53 \times 10^5$ m^2 and a three-dimensional surface area of $2{\cdot}71 \times 10^5$ m^2. The distal portion of the deposit extending beyond the edge of the active talus slope has a mean thickness of 8 m and a maximum thickness of 18 m. The deposit has a hummocky morphology and a clast-supported surface cover of large angular boulders. The distal portion of the deposit extending beyond the active talus slope displays an asymmetric topography along its

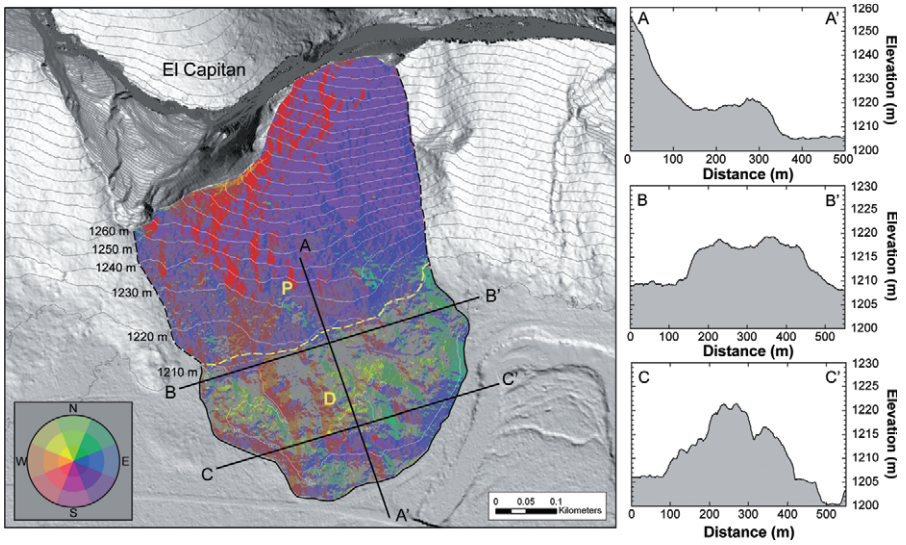

Figure 4. Slope–aspect map showing the surface morphology of the El Capitan Meadow rock avalanche. Topographic contour interval is 10 m. The dashed yellow line divides the proximal (P) and distal (D) portions of the deposit used to calculate the deposit volume. The deposit has an asymmetric longitudinal profile (A–A′) and roughly symmetrical cross-sections (B–B′ and C–C′).

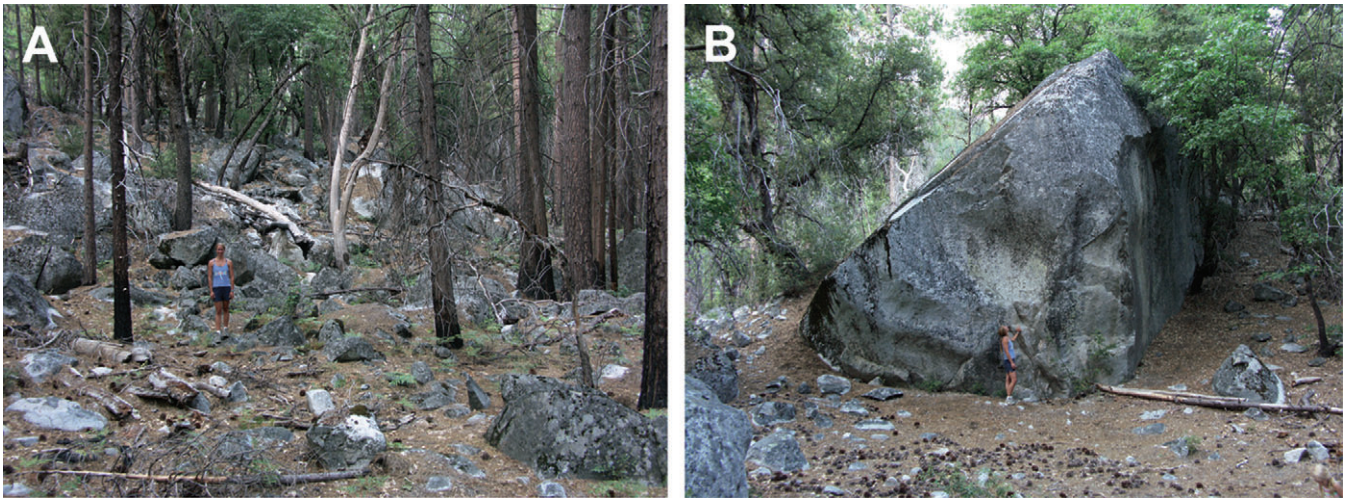

Figure 5. Surface morphology of the El Capitan Meadow rock avalanche. (A) The bouldery distal edge of deposit, showing abrupt change in slope. (B) The largest boulder along the distal edge of the rock avalanche deposit, ~2700 m^3 in volume, has a minimum dimension of ~11 m, indicating the minimum dimension of at least part of the failed rock mass. Note person for scale in both photos.

length, revealed in a slope-aspect map and in a longitudinal cross-section (Figure 4). Beyond the edge of the active talus, the deposit is relatively fine-grained and has a low topographic gradient, sloping gently upward ~6 m to the crest (Figure 4). The crest is considerably coarser, with boulders several meters in diameter. From the crest, the deposit surface slopes steeply down to the valley floor (Figure 4). This 'back-sloping' morphology suggests that the deposit is not composite from several rock-fall events. The distal portion is generally very coarse, with large angular boulders projecting several meters above the mean deposit surface (Figure 5A). The largest boulders in the deposit are clustered along the distal margin and are up to ~2700 m^3 in volume (Figure 5B).

Determining the exact volume of the rock avalanche deposit is challenging because an undetermined amount of more recent talus has accumulated on top of that portion proximal to the cliff. Because the distal portion of the rock avalanche has a distinct margin and extended out over the nearly horizontal valley floor (Figure 2), the volume for that portion is well constrained by calculating the volume of debris above a horizontal plane at 1204 m amsl (a two-dimensional surface area of $1{\cdot}03 \times 10^5$ m^2). This yields a debris volume for the distal portion of $1{\cdot}03 \times 10^6$ m^3. This calculation assumes no aggradation of the valley floor over the relatively short time span since the rock avalanche occurred (~3·6 ka; see below). Determining the volume for the proximal portion of the rock avalanche requires an assumption about the extent and thickness of the deposit beneath the active talus. Assuming a tapered wedge beneath the two-dimensional surface area ranging from 1 m thick at the base of the cliff to 8 m where the deposit first appears from beneath the active talus slope, the debris volume for the proximal portion of the rock avalanche deposit is $1{\cdot}16 \times 10^6$ m^3. Summing the two portions yields a total deposit volume of $2{\cdot}19 \times 10^6$ m^3. This estimate is less than the $3{\cdot}79 \times 10^6$ m^3 estimate reported by Wieczorek *et al.* (1999), probably due to different assumptions regarding the thickness of the rock avalanche deposit beneath the active talus slope, and perhaps also due to the enhanced resolution of the LiDAR-based DEM.

The volume of the rock avalanche deposit can be converted to an approximate volume of the intact rock mass at the source area prior to failure. Assuming a talus density of 1·80 g cm^{-3}

(Sass and Wollny, 2001; Hales and Roering, 2005) and granitic rock density of 2·65 g cm^{-3}, the porosity of active talus slope beneath El Capitan should be on the order of 30% (Moore *et al.*, 2009). We observe that the porosity of the rock avalanche deposit is somewhat less than that of the active talus slope, approximately 25%, a value that is in general agreement with other estimates of rock avalanche volume dilation (Nicoletti and Sorriso-Valvo, 1991, and references therein). Reducing the El Capitan Meadow rock avalanche deposit volume by 25% yields an intact rock volume of 1·64 $\times 10^6$ m^3.

Rock Avalanche Source Area

Due to their large volumes, rock avalanches usually have clearly defined source areas, easily identified by large scars or arcuate depressions on hillslopes (Hewitt, 2002; Ballantyne and Stone, 2004; Mitchell *et al.*, 2007). However, El Capitan is unusual in that it does not preserve an immediately obvious source area (Figure 1). The morphology of the rock avalanche deposit indicates that it was sourced from the south-east face, east of the 'Nose', the prominent arête at the center of the formation, and west of the 'North American Wall', a concave, vertical to slightly overhanging portion of the face named after a mafic dike complex in the shape of North America (Figures 1 and 6D). The width of the rock avalanche deposit constrains the maximum width of the source area to ~550 m; however, because the rock avalanche likely spread laterally across the talus slope and valley floor, the actual source area may have been much narrower.

El Capitan is characterized by a heterogeneous intrusive igneous lithology, which can be used to place further constraints on the rock avalanche source area. Previously published geologic maps show the El Capitan Granite to be the dominant rock type along the south-western flank and at the base of the south-east face, whereas the Taft Granite is prevalent on the south-eastern flank and at the summit (Calkins *et al.*, 1985; Peck, 2002; Ratajeski *et al.*, 2001). There are clear differences in grain size and mafic mineral content between these two lithologies: the El Capitan Granite is a light-colored, coarse-grained biotite granodiorite and granite containing 5–10% mafic minerals, primarily biotite, whereas the Taft Granite is a light-colored, medium-grained, equigranular leucogranite containing 1–5% biotite (Bateman, 1992; Peck, 2002). In addition to these granites, two sets of mafic dikes are exposed on the south-east face, an older, light-colored granodioritic series, and a younger, darker dioritic series whose outcrop pattern resembles the map of North America, and for which the North America Wall is named (Figure 1; Reid *et al.*, 1983; Ratajeski *et al.*, 2001). Numerous thin (<5 m) aplite dikes are also present.

A surficial geologic map (Figure 6A) of the distal portion of the rock avalanche deposit (n = 650 boulders) reveals that the surface is composed of approximately equal amounts of Taft Granite (34%), mafic dikes of the granodiorite series (29%) and El Capitan Granite (27%), with lesser amounts of the North America diorite (9%) and aplite (1%). The various lithologies are broadly distributed and well mixed throughout the distal portion of the deposit, with no clear spatial patterns (Figure 6A). Smaller boulders of El Capitan Granite and diorite become more common with proximity to the active talus slope below El Capitan, reflecting more recent deposition on the active talus after the rock avalanche occurred.

The distribution of rock types in the deposit, in particular the presence of Taft Granite (Figure 6A), can be used to place further constraints on the source area, provided the extent of these rock types on the south-east face is known. Geologic mapping combining field mapping on climbing routes and high-resolution photography (www.xrez.com/yose_proj/Yose_index.html) reveals the outcrop patterns of the various units on the south-east face. Field mapping involved scaled photography of the rock type at each 'belay' (anchor point between rope lengths) on several of the major climbing routes ascending the south-east face (n = 72, Figure 6B, 6C). These served as calibration points for more detailed mapping using the high-resolution photographs. Differences in grain size between the El Capitan and Taft granites, as well as differences in the mafic mineral content between these granites and the mafic dikes, allow for accurate delineation of contacts between these units.

A preliminary geologic map of a portion of the south-east face indicates that the Taft Granite is present as a distinct wedge-shaped outcrop below the summit of El Capitan (Figure 6D). A mafic dike of the granodiorite series forms the contact between the Taft and El Capitan granites, and includes small bodies of North America diorite. The El Capitan Granite composes the remainder of the rock within this portion of the south-east face. The outcrop pattern of these rock types, in particular the rather limited extent of Taft Granite only near the summit, constrains the potential source area for the rock avalanche to a maximum elevation of 2155 m and an approximate minimum elevation of ~1800 m (because the El Capitan Granite extends to the base of the cliff, its presence in the rock avalanche deposit does not tightly constrain the minimum elevation of the source area). Within these bounds, the approximate surface area of the rock avalanche source is 8·5 $\times 10^4$ m^2 (Figure 6D).

Dividing the volume of the intact rock mass (1·64 $\times 10^6$ m^3) by the surface area of the potential source area, i.e. assuming that the failed rock mass was distributed uniformly across the potential source area, yields a mean slab thickness of 19 m. If the rock avalanche originated from a larger area, the slab thickness would be smaller; conversely, if the rock avalanche originated from only a portion of this area, the slab thickness would be larger. Considering that the rock avalanche source area is presently nearly vertical (dipping ~87° southeast), a rock slab ≥19 m thick would have taken the form of a substantially overhanging rock mass. Although this amount of overhang may seem extreme, the rock mass strength of the granitic rocks composing El Capitan is clearly capable of supporting such structures; the face east of the North America Wall in the vicinity of the climbing route 'Tangerine Trip' (Figure 6D) presently overhangs by 37 m horizontally from the base of the cliff. Furthermore, the largest boulder in the distal portion of the rock avalanche deposit (Figure 5B) has a minimum dimension of ~11 m. This represents a minimum thickness for at least part of the rock mass prior to failure (a minimum value because the boulder probably fragmented from a larger rock mass upon impacting the talus slope), supporting the notion of planar or slab failure of a relatively thick rock mass.

Rock Avalanche Dynamics

Identifying the potential rock avalanche source area provides insight into the dynamics of the fall and resulting runout. Qualitatively, after detachment the rock mass fell ~650 m down the cliff face, losing potential energy (Figure 7). During the initial fall the rock mass rapidly accelerated due to gravity, with minimal frictional deceleration due to the near vertical cliff angle. The rock mass fragmented upon impact with the apex of the talus slope, causing the various lithologies to

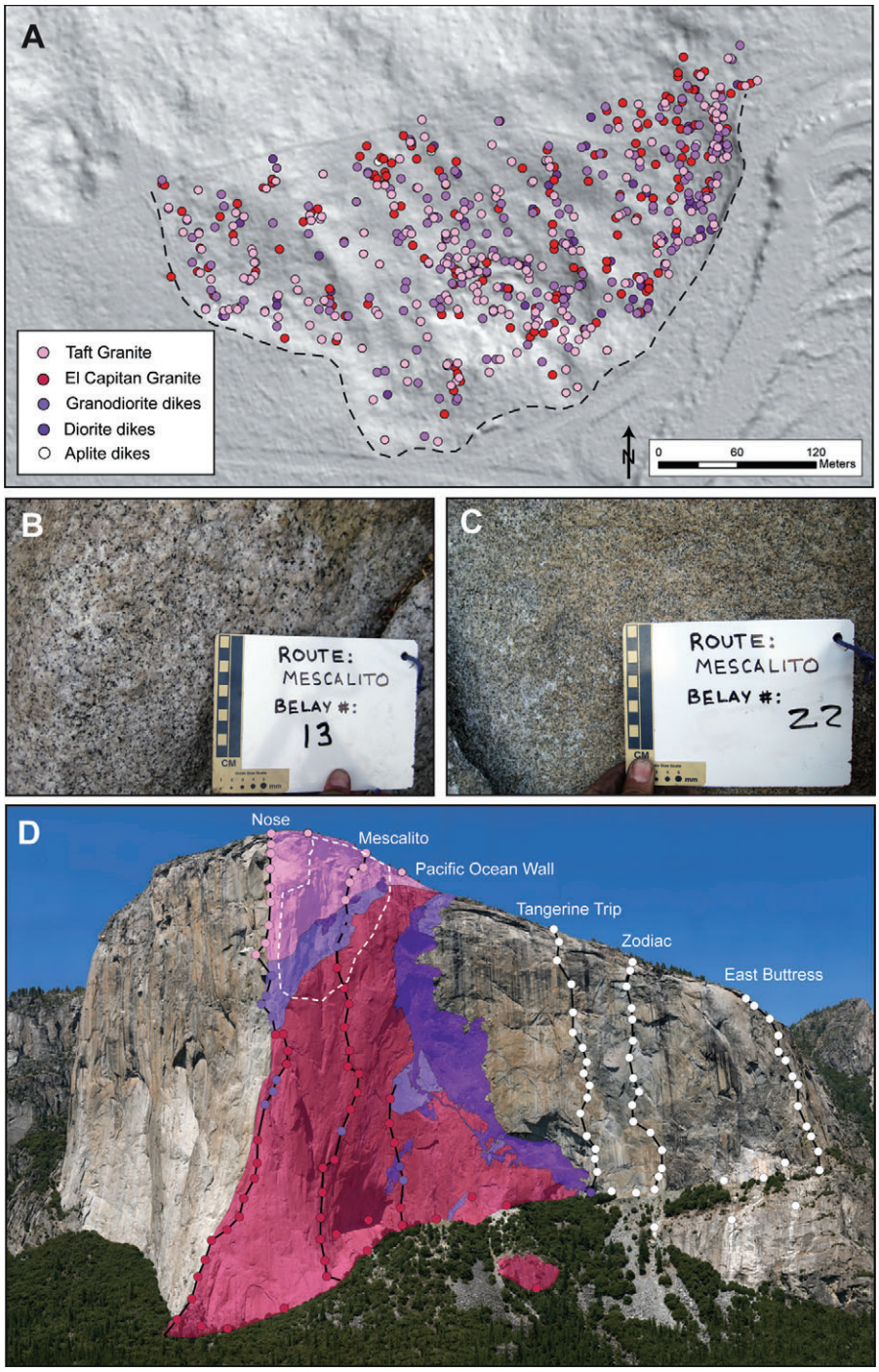

Figure 6. Lithologic constraints on the El Capitan Meadow rock avalanche source area. (A) Distribution of rock types on the surface of the deposit, showing roughly equal proportions of Taft Granite, El Capitan Granite, and the granodiorite dike series. The El Capitan Granite (B) and granodiorite dike series (C) as mapped on the cliff face. (D) Preliminary geologic map of the south-east face, between the Nose and the North America Wall, showing outcrop patterns. Black lines mark climbing routes, colored circles mark mapping locations (white circles mark mapping locations that were not included in this map), and the white dashed line delineates the approximate rock avalanche source area.

become well mixed (Figure 6A). Vertical momentum was transferred to horizontal momentum as the debris traveled down the talus slope, dipping south east at a mean angle of 23°, for approximately 395 m to the valley floor (Figure 7). The debris mass was topographically unconfined, with free downward and lateral expansion of the debris across the talus slope and valley floor. As the rock debris moved down the talus slope, the rate of energy dissipation by basal and internal friction became greater than the rate of supply of potential energy. On reaching the flat valley floor the rock mass ceased to lose potential energy, but continued forward due to stored kinetic energy until the last of the kinetic energy was dissipated by friction and the rock mass stopped. This spontaneous stopping led to compression of the distal portion of the rock avalanche deposit, producing the 'back-sloping' morphology (Figure 4).

Quantitatively, we determined the maximum velocity and energy balance of the falling rock mass using an algorithm similar to that reported by Wieczorek *et al.* (2000), which numerically integrates the acceleration due to gravity and deceleration due to friction of a distributed mass in two dimensions (x, y; Figure 7). We modified this algorithm to calculate the average tangential velocity, and also the energy balance in terms of the percentage of potential, kinetic, and

dissipated energy, as a function of time and tangential distance (Figure 8). We performed the calculation on an elevation profile representing the travel path from the inferred centroid of the source area to the inferred toe of the debris deposit (Figure 7). The apparent coefficient of kinetic friction (or kinetic frictional resistance), $\mu_\kappa = 1{\cdot}01$, was chosen such that the velocity is zero at the distal edge of the rock avalanche deposit. This coefficient lumps all the mechanisms that act to decelerate the avalanche (e.g. energy dissipation by friction, transformation to thermal and acoustic energy, etc.) into one parameter, and is assumed constant and independent of the tangential velocity, although in practice μ_κ probably deceases with increasing tangential velocity.

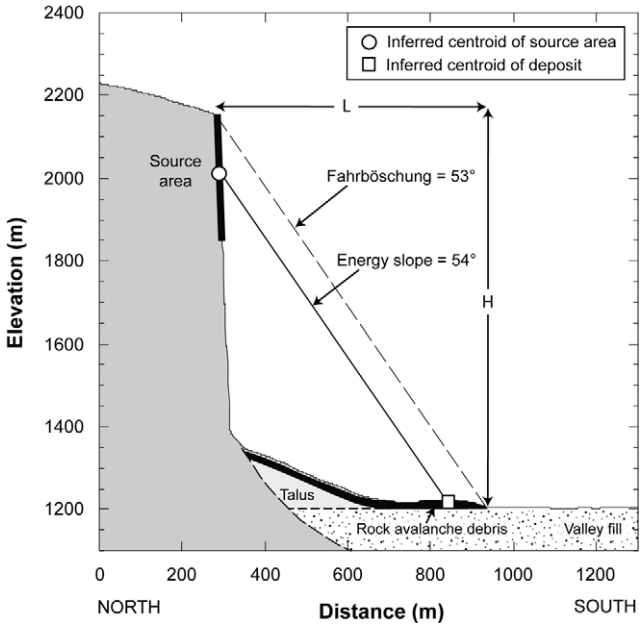

Figure 7. Profile of the El Capitan Meadow rock avalanche. The rock avalanche source area and extent of deposit are shown in black, inferred where underneath talus. Subsurface bedrock contact from Gutenberg *et al.* (1956).

The model calculates the tangential velocity, and the partitioning between potential, kinetic, and dissipated energy, as a function of tangential distance and total elapsed time (Figure 8). Assuming instantaneous detachment, the maximum velocity for the rock avalanche calculated by this method is 101 ± 0·5 m s^{-1} (safely assumed to be 100 m s^{-1}), and it is reached 11·7 s after detachment at a tangential distance of 656 m from the centroid of the source area, where the kinetic energy maxima is also achieved (Figure 8). The total emplacement time is calculated to be 24·1 s (Figure 8). The maximum velocity determined by this method is similar to that determined using an energy slope approach (Hungr *et al.*, 2005; Dortch *et al.*, 2009), in which the maximum vertical distance between the inferred original topography and a line connecting the centroid of the source area with the centroid of the deposit is used to calculate the velocity attained by gravitational acceleration (Figure 7). An energy slope (53°; Figure 7) approach yields a maximum velocity for the El Capitan rock avalanche of 108 m s^{-1}.

Rock avalanche dynamics are often evaluated through use of the Fahrböschung (Heim, 1932), the angle of a line connecting the top of the source area to the most distal part of the deposit (Figure 7), and through the ratio of the maximum fall height (*H*) to the maximum runout distance (*L*). These metrics are useful for comparing different rock avalanches, but can greatly overestimate rock avalanche velocities (Hutchinson, 2006). The relatively steep Fahrböschung angle for the El Capitan Meadow rock avalanche (54°; Figure 7) confirms the steep gradient of energy loss and short transport distance. The *H*/*L* ratio is 1·34 (Table 1), considerably larger than most reported rock avalanches, which are typically in the range of 0·1–0·6. Energy loss during impact at the base of the cliff substantially reduced the energy available for horizontal motion. Thus, the El Capitan Meadow rock avalanche does not appear to be an example of 'excessive runout' landslide, or sturzstrom (Hsu, 1975; Nicoletti and Sorriso-Valvo, 1991; Davies and McSaveney, 1999). Rather, the deposit extended out onto the floor of Yosemite Valley primarily because of its great potential energy (total potential vertical fall distance of ~950 m), low initial friction, and topographically unconfined travel path.

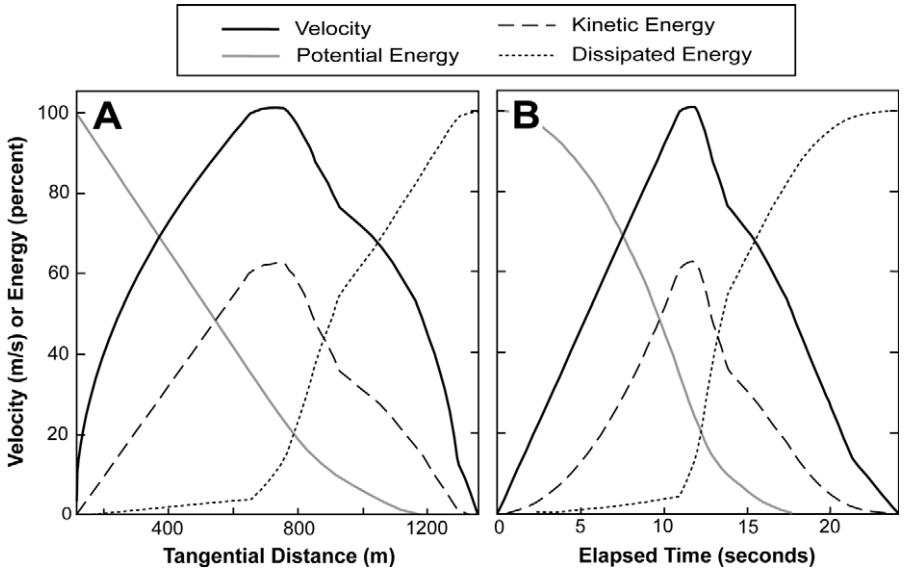

Figure 8. Tangential velocity and fraction of potential, kinetic, and dissipated energies as a function of (A) tangential distance of the falling rock mass and (B) total elapsed time. The tangential distance starts at 112 m (the distance from the top of the potential source area to the centroid of the distributed mass). The slope breaks in the velocity, kinetic energy, and dissipated energy correspond to the slope breaks in the rock avalanche profile (Figure 7). The final slope break in the tangential velocity at approximately 1280 m tangential distance corresponds to the maximum thickness of the rock avalanche deposit.

Age of the El Capitan Meadow Rock Avalanche

Determining the age of the El Capitan Meadow rock avalanche is critical for evaluating possible triggering mechanisms, e.g. post-glacial stress changes, meteorological events, or seismic strong ground motion. Cosmogenic ^{10}Be exposure dating of a prominent recessional moraine and of the rock avalanche itself (Figure 2) constrains the timing of failure. These deposits are generally well suited for cosmogenic exposure dating because the processes that form them tend to quickly excavate rocks before exposing them on the surface; this is particularly true for rock avalanches, making them an appealing target for exposure dating (Ivy-Ochs *et al.*, 1998, 2009; Barnard *et al.*, 2001; Ballantyne and Stone, 2004; Mitchell *et al.*, 2007; Dortch *et al.*, 2009). Vertical cliffs receive relatively low doses of cosmic rays due to topographic shielding, and the great volumes of rock avalanches suggest that most boulders now exposed on the surface were shielded deep within the cliff prior to failure. Nevertheless, geomorphic deposits must be carefully sampled to ensure reliable exposure dates. Complicating factors can include pre-failure cosmic ray exposure, erosion of the deposit, rotation of boulders after deposition, rock spallation due to forest fires, and topographic, vegetation, and snow shielding of cosmic rays (Bierman and Gillespie, 1991; Gosse and Phillips, 2001; Putkonen and Swanson, 2003; Ivy-Ochs *et al.*, 2009). To address those issues, we collected moraine samples from the tallest boulders on the crest of the moraine, minimizing the effects of erosional degradation (Putkonen and Swanson, 2003). We collected rock avalanche samples from clast-supported, boulder-dominated areas and sampled boulders that were wedged in the deposit and hence could not have rotated since deposition. We minimized the potential for fire-induced rock spallation by sampling only the tops of large boulders. We conducted detailed surveys of the topographic shielding, which is significant beneath the ~1 km tall cliffs (Table II), but determined that snow and vegetation shielding are negligible at this location. We assumed a boulder erosion rate of 0·0006 cm yr^{-1}, a typical value for granitic boulders and bare bedrock surfaces in the Sierra Nevada (Small *et al.*, 1997; Stock *et al.*, 2005).

The glacial history of Yosemite Valley provides a first-order constraint on the age of the El Capitan Meadow rock avalanche: the deposit must post-date glacial occupation of the valley below El Capitan, for any rock debris falling onto the glacier would have been transported to the terminal moraine several kilometers down the valley. Cosmogenic ^{10}Be concentrations in three large boulders on the crest of the El Capitan recessional moraine, located 850 m down valley from the rock avalanche deposit (Figure 2), yield exposure ages between 16·4 and 23·5 ka, with a mean age of 19·8 ka (Table II). This age is consistent with previous estimates for the Tioga glaciation (Phillips *et al.*, 1996; 2009; Clark *et al.*, 2003). LGM deglaciation likely occurred rapidly in the Yosemite region (Clark *et al.*, 2003), with the area around El Capitan probably becoming ice-free by ~15–17 ka. Thus, the El Capitan Meadow rock avalanche must be younger than ~15–17 ka.

Four of the five sampled boulders on the rock avalanche deposit yield ^{10}Be exposure ages clustered between 3·50 and 3·84 ka, within analytical uncertainty, and yield an error weighted mean age of 3·6 ± 0·2 ka (Table II). These samples span the width of the deposit, indicating that it either resulted from a single event or from multiple events relatively closely spaced in time (i.e. within the analytical uncertainty in the data). A fifth boulder yields a much older age of 21·9 ka (Table II). This age represents a clear outlier from the other samples, and is at odds with the deglaciation history described above. Exposure ages from the El Capitan recessional moraine suggest that it is unlikely that even a portion of the rock avalanche occurred at 21·9 ka because the LGM glacier probably still occupied the flank of El Capitan at that time. The 21·9 ka exposure age does not appear to represent the timing of failure, and instead results from inherited nuclide concentration due to exposure on the cliff prior to occurrence of the rock avalanche (Ivy-Ochs *et al.*, 2009), i.e. the sampled boulder surface was at or near the cliff face prior to failure. This result confirms the need to collect and analyze multiple samples from each deposit to be dated (Putkonen and Swanson, 2003), even for deposits, such as rock avalanches, that have relatively simple depositional histories. Excluding the 21·9 ka outlier age yields an otherwise consistent age of ~3·6 ka for the El Capitan Meadow rock avalanche.

Destabilizing Factors and Possible Triggering Mechanism(s)

Post-glacial adjustment of rock slopes reflects the interaction of changing stress conditions, resulting from glacial oversteepening and relaxation of residual stresses following debutressing, and rock mass strength, controlled by lithology and discontinuities (Ballantyne, 2002). Studies of rock slopes in formerly glaciated areas suggest that oversteepened slopes

Table II. Cosmogenic beryllium-10 data and exposure ages for El Capitan moraine and rock avalanche boulders

Sample	Deposit type	Latitude	Longitude	Elevation (m amsl)	Mass qtz (g)	^{10}Be/^{9}Be (10^{-15})[a]	Shielding	P_{10} (atm g^{-1} yr^{-1})[b]	^{10}Be (10^{4} atm g^{-1}/qtz)	Exposure age (ka)[c]
ECM-1	Moraine	37·7228081	–119·643703	1215	20·25	237·40 ± 33·52	0·8884	9·81	22·69 ± 3·37	23·53 ± 4·59
ECM-2	Moraine	37·7227539	–119·643701	1216	55·70	535·00 ± 18·68	0·8884	9·74	18·92 ± 6·83	19·37 ± 2·02
ECM-3	Moraine	37·7231261	–119·643987	1216	43·37	359·30 ± 27·63	0·8884	9·58	16·02 ± 1·28	16·43 ± 2·11
ECL-1	Rock avalanche	37·7253064	–119·633139	1219	36·19	69·31 ± 7·93	0·8609	9·39	3·84 ± 0·59	3·78 ± 0·68
ECL-3	Rock avalanche	37·7254811	–119·632579	1221	38·08	66·25 ± 3·71	0·8557	9·38	3·55 ± 0·32	3·49 ± 0·45
ECL-4	Rock avalanche	37·7260069	–119·632835	1211	36·89	69·62 ± 6·13	0·8622	9·38	3·83 ± 0·47	3·77 ± 0·58
ECL-6	Rock avalanche	37·7265083	–119·630959	1214	42·30	347·80 ± 46·57	0·8457	9·27	20·15 ± 2·82	21·94 ± 4·06
ECL-8	Rock avalanche	37·7252681	–119·634443	1211	34·05	60·66 ± 7·27	0·8609	9·33	3·50 ± 0·59	3·46 ± 0·67

[a] ^{10}Be/^{9}Be ratios normalized to NIST standards (Nishiizumi *et al.*, 2007). Uncertainty is 1σ analytical uncertainty.
[b] Local ^{10}Be production rate, incorporating spallogenic and muogenic production scaled for latitude, altitude, and topographic shielding (Balco *et al.*, 2008).
[c] Exposure ages calculated using the CRONUS calculator (Balco *et al.*, 2008) and assuming a ^{10}Be half-life of 1·36 ± 0·07 Myr (Nishiizumi *et al.*, 2007), an attenuation length scale of 160 g cm^{-2}, rock density of 2·65 g cm^{-3}, and the spallation scaling scheme of Lal (1991) and Stone (2000).

tend to adjust rapidly to these stress changes by rock mass failure, but that the timing and magnitude of these failures are strongly controlled by rock mass strength (Augustinus 1995a,b). The vertical to overhanging face of El Capitan has clearly been steepened by glacial erosion, but the timing of the rock avalanche and the approximate location of the source area suggest that it did not fail in response to stress release associated with deglaciation. Although rock mass failures related to debutressing may lag deglaciation by centuries or even millennia (Ballantyne, 2002; Ballantyne and Stone, 2004), the ~13 kyr lag between deglaciation of Yosemite Valley and failure of the El Capitan Meadow rock avalanche suggests other triggering mechanisms. As described above, the El Capitan Meadow rock avalanche appears to have originated from near the summit of El Capitan, which is well above the LGM limit and has probably not been glaciated in at least 800,000 years (Huber, 1987). Large rock falls tend to be more common from the upper slopes of Yosemite Valley, above the limit of LGM glaciation, where rocks tend to be more weathered (Wieczorek *et al.*, 1999; Wieczorek, 2002). However, we note that the rocks composing the upper south-east face of El Capitan are only slightly weathered. Intersections between surface parallel sheeting joints and vertically oriented discontinuities, which are more prevalent in the Taft Granite, likely formed zones of weakness along which detachment occurred. In addition, lithologic contacts and dikes within the source area (Figure 6D) may have helped to destabilize the rock mass; for example, Weidinger and Korup (2009) determined that leucogranite dikes in the source area contributed to a large rock slope failure in the Himalaya.

Triggering of large rock slope failures is often attributed to thresholds associated with either intense precipitation events (Wieczorek, 2002; Malamud *et al.*, 2004; Gabet *et al.*, 2004) or large magnitude earthquakes (Keefer, 1984, 1994; Barnard *et al.*, 2001; Wieczorek, 2002; Malamud *et al.*, 2004; Strom and Korup, 2006; Owen *et al.*, 2008; Yin *et al.*, 2009); note, however, that rock avalanches have also been shown to occur in the absence of any obvious triggering mechanisms (McSaveney, 2002). It is difficult to evaluate the potential role of an extreme precipitation event in triggering the El Capitan Meadow rock avalanche because of uncertainty in both the exposure dating of the deposit and in the chronology of local paleoclimate records. Moreover, intense but short duration precipitation events may not be preserved well in the geologic record. Existing geologic and paleoclimate data do not record such an event, nor do they suggest an abnormally wet climate in the Yosemite region during the mid- to late-Holocene; rather, this period was more notable for persistent droughts (Brunelle and Anderson, 2003; Mensing *et al.*, 2004). Without clear evidence for an intense precipitation event in the central Sierra Nevada circa 3·6 ka, a climatic trigger for the El Capitan Meadow rock avalanche is equivocal.

As described above, earthquakes on and adjacent to the Sierra Nevada frontal fault system, and also possibly on the San Andreas Fault (Figure 1 inset), have triggered numerous rock falls in the Sierra Nevada (Harp *et al.*, 1984; Keefer, 1994; Bull *et al.*, 1994; Wieczorek and Snyder, 2004). Recall that the AD 1872 Owens Valley earthquake in the south-eastern Sierra Nevada triggered numerous large (up to 36 000 m^3) rock falls in Yosemite Valley (Wieczorek and Snyder, 2004). Lee *et al.* (2001) investigated offset strata in trenches across the southern Owens Valley fault zone and, based on optically stimulated luminescence dating, concluded that the pre-1872 (penultimate) Owens Valley fault rupture occurred sometime between 3·3 ± 0·3 and 3·8 ± 0·3 ka. ^{10}Be exposure dates for the El Capitan Meadow rock avalanche reported here fall within this range, providing a plausible link to the penultimate Owens Valley fault earthquake. The magnitude–volume relationships of Malamud *et al.* (2004) and the magnitude–landslide distance relationships of Keefer (1984) suggest that this earthquake should have had a magnitude of ~M7.0 or greater. Factors related to the earthquake, including rupture depth, direction of energy focusing, and regional attenuation, as well as other factors such as topography, lithology, discontinuity spacing and orientation, and the hydrological conditions at the time of failure may have influenced the minimum magnitude and distance required to trigger the rock avalanche (Malamud *et al.*, 2004). Subsequent work on the southern Owens Valley fault segment by Bacon and Pezzopane (2007) suggests that the 3·3–3·8 ka rupture identified by Lee *et al.* (2001) may have instead occurred on the northern Owens Valley fault segment and/or on the southern White Mountains fault zone. If correct, this would put the epicenter of faulting closer to Yosemite Valley, increasing local ground shaking there.

Ultimately we cannot exclude the possibility of a non-seismic triggering mechanism such as an intense precipitation event for the El Capitan Meadow rock avalanche; indeed, such precipitation events are known to have triggered historic large rock slope failures in the Sierra Nevada (Wieczorek, 2002). Furthermore, many large rock falls and rock slides in Yosemite have occurred in the absence of recognized triggering mechanisms (e.g. the 10 March 1987 Middle Brother rock fall of ~600,000 m^3; Wieczorek and Snyder, 2004). However, the very large volume of the El Capitan Meadow rock avalanche deposit, the convergence of exposure dates with the estimated timing of the penultimate rupture of the Owens Valley fault, and the fact that the AD 1872 Owens Valley fault earthquake generated very large rock falls in Yosemite Valley, all support a seismic trigger. Matthes (1930) may well have been correct in describing the El Capitan Meadow rock avalanche deposit as an 'earthquake avalanche'.

There are at least five other large rock fall deposits in Yosemite Valley that have been interpreted as rock avalanches, including one near Mirror Lake in eastern Yosemite Valley with a much larger volume that of the El Capitan Meadow rock avalanche (~$11{\cdot}4 \times 10^6$ m^3; Wieczorek *et al.*, 1999; Wieczorek, 2002). Given the large size of these deposits, it is plausible that they too were triggered by earthquakes, and perhaps by the ~3·6 ka Owens Valley and/or White Mountain faulting event. Additional ^{10}Be exposure dating of these deposits will help to test this hypothesis. If these rock avalanches are also found to coincide with seismic events, it would suggest that the extreme hazard posed by rock avalanches in Yosemite Valley remains present and depends on local earthquake recurrence intervals, emphasizing the need for detailed paleoseismic data from the Sierra Nevada frontal fault system and adjacent faults.

Conclusions

The morphology and age of the $2{\cdot}19 \times 10^6$ m^3 El Capitan Meadow rock avalanche deposit in Yosemite Valley indicates a massive failure of a large expanse of the south-eastern face of El Capitan. Geologic mapping of the deposit and of the south-east face constrains the source of the rock avalanche to an area near the summit of ~$8{\cdot}5 \times 10^4$ m^2. The rock mass free fell ~650 m, attaining a maximum velocity of 100 m s^{-1} before impacting the talus slope and spreading across the valley floor. Four cosmogenic beryllium-10 exposure ages from boulders in the deposit are tightly clustered between 3·5 and 3·8 ka, with a mean age of 3·6 ± 0·2 ka. These samples span the width of the deposit, confirming that it resulted from a single event.

A fifth boulder gives a much older age of 21·9 ka, at odds with the glacial history of Yosemite Valley and likely resulting from inherited nuclide concentration due to exposure on the cliff prior to failure. Because the rock avalanche occurred well after deglaciation, glacial debutressing is an unlikely trigger. However, the age of the El Capitan Meadow rock avalanche coincides with estimated rupture of the Owens Valley fault between 3·3 and 3·8 ka. This coincidence of ages, combined with the fact that the AD 1872 Owens Valley earthquake triggered numerous large rock falls in Yosemite Valley, suggest that a large magnitude (≥M7.0) earthquake centered in the south-eastern Sierra Nevada *ca* 3·6 ka may have triggered the El Capitan Meadow rock avalanche. If correct, this suggests that the hazard posed by rock avalanches in Yosemite Valley remains present and depends on local earthquake recurrence intervals.

Acknowledgements—We gratefully acknowledge the assistance of Jesse McGahey, Lincoln Else, Colter Chisum, Roger Putnam, and Holly Beck in mapping the south-east face of El Capitan, Miquela Ingalls and Daven Quinn in mapping the rock avalanche deposit, and Allen Glazner and Bryan Law in rock identification. We appreciate constructive comments from Johannes Weidinger, Oliver Korup, and an anonymous reviewer. ^{10}Be analyses were provided by Purdue Rare Isotope Measurement (PRIME) laboratory at Purdue University as part of the free seed analysis program.

References

Augustinus PC. 1995a. Rock mass strength and the stability of some glacial valley slopes. *Zeitschrift für Geomorphologie* **39**: 55–68.

Augustinus PC. 1995b. Glacial valley cross-profile development: the influence of in situ rock stress and rock mass strength, with examples from the Southern Alps, New Zealand. *Geomorphology* **14**: 87–97.

Bacon SN, Pezzopane SK. 2007. A 25,000-year record of earthquakes on the Owens Valley fault near Lone Pine, California: implications for recurrence intervals, slip rates, and segmentation models. *Geological Society of America Bulletin* **119**: 823–847; doi: 10.1130/B25879.1.

Balco G, Stone JO, Lifton NA, Dunai TJ. 2008. A complete and easily accessible means of calculating surface exposure ages or erosion rates from ^{10}Be and ^{26}Al measurements. *Quaternary Geochronology* **3**: 174–195.

Ballantyne CK. 2002. Paraglacial geomorphology. *Quaternary Science Reviews* **21**: 1935–2017.

Ballantyne CK, Stone, JO. 2004. The Beinn Alligin rock avalanche, NW Scotland: Cosmogenic ^{10}Be dating, interpretation and significance. *The Holocene* **14**: 448–453.

Barnard PL, Owen LA, Sharma MC, Finkel RC. 2001. Natural and human-induced landsliding in the Garhwal Himalaya of Northern India. *Geomorphology* **40**: 21–35.

Bateman PC. 1992. Plutonism in the central part of the Sierra Nevada batholith, California. US Geological Survey Professional Paper 1483.

Beanland S, Clark MM. 1994. The Owens Valley fault zone, eastern California, and surface rupture associated with the 1872 earthquake. US Geological Survey Bulletin 1982.

Bierman PR, Gillespie A. 1991. Range fires: a significant factor in exposure-age determination and geomorphic surface evolution. *Geomorphology* **19**: 641–644.

Brunelle A, Anderson RS. 2003. Sedimentary charcoal as an indicator of late-Holocene drought in the Sierra Nevada, California, and its relevance to the future. *The Holocene* **13**: 21–28.

Bull WB, King J, Kong F, Moutoux T, Phillips WM. 1994. Lichen dating of coseismic landslide hazards in alpine mountains. *Geomorphology* **10**: 253–264.

Calkins FC, Huber NK, Roller JA. 1985. Geologic bedrock map of Yosemite Valley, Yosemite National Park, California. US Geological Survey Map I-1639.

Clark D, Gillespie AR, Clark M, Burke R. 2003. Mountain glaciations of the Sierra Nevada. In *Quaternary Geology of the United States*, Easterbrook DJ (ed). INQUA Field Guide Volume, Desert Research Institute: Reno, Nevada; 287–311.

Davies TR, McSaveney MJ. 1999. Runout of dry granular avalanches. *Canadian Geotechnical Journal* **36**: 313–320.

Dortch JM, Owen LA, Haneberg WC, Caffee MW, Dietsch C, Kamp U. 2009. Nature and timing of large landslides in the Himalaya and Transhimalaya of northern India. *Quaternary Science Reviews* **28**: 1037–1054, doi: 10.1016/j.quascirev.2008.05.002

Gabet EJ, Burbank DW, Putkonen JK, Pratt-Situala BA, Ojha T. 2004. Rainfall thresholds for landsliding in the Himalaya of Nepal. *Geomorphology* **63**: 131–143.

Gosse JC, Phillips FM. 2001. Terrestrial in situ cosmogenic nuclides: theory and application. *Quaternary Science Reviews* **20**: 1475–1560.

Gutenberg B, Buwalda JP, Sharp RP. 1956. Seismic explorations on the floor of Yosemite Valley, California. *Geological Society of America Bulletin* **67**: 1051–1078.

Hales TC, Roering JJ. 2005. Climate-controlled variations in scree production, Southern Alps, New Zealand. *Geology* **33**: 701–704.

Harp EL, Tanaka K, Sarmiento J, Keefer DK. 1984. Landslides from the May 25–27, 1980, Mammoth Lakes, California, earthquake sequence. US Geological Survey Miscellaneous Investigations Series Map I-1612.

Heim A. 1932. *Bergsturz und Menschenleben*. Fretz and Wasmuth: Zurich.

Hewitt K. 2002. Styles of rock avalanche depositional complexes conditioned by very rugged terrain, Karakoram Himalaya, Pakistan. In *Catastrophic Landslides*: *Effects, Occurrence and Mechanisms*, Evans SG, DeGraff J (eds). Geological Society of America, Reviews in Engineering Geology XV; 345–377.

Hovius N, Stark CP. 2007. Landslide-driven erosion and topographic evolution of active mountain belts. In *Landslides from Massive Rock Slope Failure*, Evans SG, Mugnzza GS, Strom A, Hermanns RL (eds). Springer: Netherlands; 573–590.

Hsu KJ. 1975. On sturzstroms – catastrophic debris streams generated by rockfalls. *Geological Society of America Bulletin* **86**: 129–140.

Huber NK. 1987. The Geologic Story of Yosemite National Park. US Geological Survey Bulletin 1595.

Hungr O, Coromina J, Eberhardt E. 2005. Estimating landslide motion mechanism, travel distance and velocity. In *Landslide Risk Management*, Hungr O, Fell R, Couture R, Eberhardt E (eds). Taylor & Francis: London; 99–128.

Hutchinson JN. 2006. Massive rock slope failure: perspectives and retrospectives on state-of-the-art. In *Landslides from Massive Rock Slope Failure*, Evans SG, Mugnozza GA, Strom A, Hermans RL (eds). Springer: Netherlands; 619–662.

Ivy-Ochs S, Heuberger H, Kubik PW, Kerschner H, Bonani G, Frank M, Schluchter C. 1998. The age of the Koefels event: relative, ^{14}C, and cosmogenic isotope dating of an early Holocene landslide in the Central Alps (Tyrol, Austria). *Zeitschrift fur Gletscherkunde und Glazialgeologie* **134**: 57–70.

Ivy-Ochs S, Poschinger AV, Synal H-A, Maisch M. 2009. Surface exposure dating of the Flims landslide, Graubünden, Switzerland. *Geomorphology* **103**: 104–112; doi: 10.1016;j.geomorph.2007.10.024

Keefer DK. 1984. Landslides caused by earthquakes. *Geological Society of America Bulletin* **95**: 406–421.

Keefer DK. 1994. The importance of earthquake-induced landslides to long-term slope erosion and slope-failure hazards in seismically active regions. *Geomorphology* **10**: 265–284.

Korup O, Clague JJ, Hermanns RL, Hewitt K, Strom AL, Weidinger JT. 2007. Giant landslides, topography, and erosion. *Earth and Planetary Science Letters* **261**: 578–589.

Lal D. 1991. Cosmic ray labeling of erosion surfaces: in situ nuclide production rates and erosion models. *Earth and Planetary Science Letters* **104**: 424–439.

Lee J, Spencer J, Owen L. 2001. Holocene slip rates along the Owens Valley fault, California: implications for the recent evolution of the Eastern California Shear Zone. *Geology* **29**: 819–822.

Malamud BD, Turcotte DL, Guzzetti F, Reichenbach P. 2004. Landslides, earthquakes, and erosion. *Earth and Planetary Science Letters* **229**: 45–49.

Matthes FE. 1930. Geologic history of the Yosemite Valley: US Geological history of the Yosemite Valley. US Geological Professional Paper 504.

McSaveney MJ. 2002. Recent rockfalls and rock avalanches in Mount Cook National Park, New Zealand. In *Catastrophic Landslides: Effects, Occurrence and Mechanisms*, Evans SG, DeGraff J (eds). Geological Society of America Reviews in Engineering Geology XV; 345–377.

Mensing SA, Benson LV, Kashgarian M, Lund S. 2004. A Holocene pollen record of persistent droughts from Pyramid Lake, Nevada, USA. *Quaternary Research* **62**: 29–38.

Mitchell WA, McSaveney MJ, Zondervan A, Kim K, Dunning SA, Taylor PJ. 2007. The Keylong Serai rock avalanche, NW Indian Himalaya: geomorphology and palaeoseismic implications. *Landslides* **4**: 245–254, doi: 10.1007/s10346-007-0085-0.

Moore J, Saunders J, Dietrich W, Glaser SD. 2009. Influence of rock mass strength on the erosion rate of alpine cliffs: *Earth Surface Processes and Landforms* **34**: 1339–1352.

Muir J. 1912. *The Yosemite: New York*. The Century Company.

Nicoletti PG, Sorriso-Valvo M. 1991. Geomorphic controls on the shape and mobility of rock avalanches. *Geological Society of America Bulletin* **103**: 1365–1373.

Nishiizumi K, Imamura M, Caffee MW, Southon JR, Finkel RC, McAninch J. 2007. Absolute calibration of ^{10}Be AMS standards. *Nuclear Instruments and Methods in Physics B* **258**: 403–413.

Owen LA, Kamp U, Khattak GA, Harp EL, Keefer DK, Bauer MA. 2008. Landslides triggered by the 8 October 2005 Kashmir earthquake. *Geomorphology* **94**: 1–9, doi: 10.1016/j.geomorph.2007.04.007.

Peck DL. 2002. Geologic map of the Yosemite Quadrangle, central Sierra Nevada, California. Geologic Investigations Series Map I-2751.

Phillips FM, Zreda MG, Benson LV, Plummer MA, Elmore D, Sharma P. 1996. Chronology for fluctuations in late Pleistocene Sierra Nevada glaciers and lakes. *Science* **274**: 749–761.

Phillips FM, Zreda M, Plummer MA, Elmore D, Clark DH. 2009. Glacial geology and chronology of Bishop Creek and vicinity, eastern Sierra Nevada, California. *Geological Society of America Bulletin* **121**: 1013–1033; doi: 10.1130/B26271.1

Putkonen J, Swanson T. 2003. Accuracy of cosmogenic ages for moraines. *Quaternary Research* **59**: 255–261.

Ratajeski K, Glazner AF, Miller BV. 2001. Geology and geochemistry of mafic to felsic plutonic rocks in the Cretaceous intrusive suite of Yosemite Valley, California. *Geological Society of America Bulletin* **113**: 1486–1502.

Reid JB, Evans OC, Fates DG. 1983. Magma mixing in granitic rocks of the central Sierra Nevada, California. *Earth and Planetary Science Letters* **66**: 243–261.

Sass O, Wollny K. 2001. Investigations regarding alpine talus slopes using ground-penetrating radar (GPR) in the Bavarian Alps, Germany. *Earth Surface Processes and Landforms* **26**: 1071–1086, doi: 10.1002/esp.254.

Scheidegger AE. 1973. On the prediction and reach of velocity of catastrophic landslides. *Rock Mechanics* **5**: 231–236.

Shea T, van Wyk de Vries B. 2008. Structural analysis and analogue modeling of the kinematics and dynamics of rockslide avalanches. *Geosphere* **4**: 657–686, doi: 10.1130/GES00131.1

Shreve RL. 1968. The Blackhawk landslide. *Geological Society of America Special Paper* **108**: 1–47.

Small EE, Anderson RS, Repka JL, Finkel R. 1997. Erosion rates of alpine bedrock summit surfaces deduced from in situ ^{10}Be and ^{26}Al. *Earth and Planetary Science Letters* **150**: 413–425.

Stock GM, Anderson RS, Finkel RC. 2005. Rates of erosion and topographic evolution of the Sierra Nevada, California, inferred from cosmogenic ^{26}Al and ^{10}Be concentrations. *Earth Surface Processes and Landforms* **30**: 985–1006.

Stone JO. 2000. Air pressure and cosmogenic isotope production. *Journal of Geophysical Research* **105**: 23753–23759.

Strom AL, Korup O. 2006. Extremely large rockslides and rock avalanches in the Tien Shan mountains, Kyrgystan. *Landslides* **3**: 125–136, doi: 10.1007/s10346-005-0027-7.

Weidinger JT, Korup O. 2009. Frictionite as evidence for a large Late Quaternary rockslide near Kachenjunga, Sikkim Himilayas, India – implications for extreme events in mountain relief destruction. *Geomorphology* **103**: 57–65, doi: 10.1016/j.geomorph.2007.10.021.

Wieczorek GF. 2002. Catastrophic rockfalls and rockslides in the Sierra Nevada, USA. In *Catastrophic Landslides: Effects, Occurrence and Mechanisms*, Evans SG, DeGraff J (eds). Geological Society of America Reviews in Engineering Geology XV; 165–190.

Wieczorek GF, Jäger S.1996. Triggering mechanisms and depositional rates of postglacial slope-movement processes in the Yosemite Valley, California. *Geomorphology* **15**: 17–31.

Wieczorek GF, Morrissey MM, Iovine G, Godt J. 1999. Rock-fall potential in the Yosemite Valley, California. US Geological Survey Open-file Report 99–578.

Wieczorek GF, Snyder JB, Waitt RB, Morrissey MM, Uhrhammer RA, Harp EL, Norris RD, Bursik MI, Finewood LG. 2000. Unusual July 10, 1996 rock fall at Happy Isles, Yosemite National Park, California. *Geological Society of America Bulletin* **112**: 75–85.

Wieczorek GF, Snyder JB. 2004. Historical Rock Falls in Yosemite National Park, California. US Geological Survey Open-File Report 03–491.

Yin Y, Wang F, Sun P. 2009. Landslide hazards triggered by the 2008 Wenchuan earthquake, Sichuan, China. *Landslides* **6**: 139–152, doi: 10.1007/s10346-009-0148-5.